SCIENTIFIC PAPERS
OF THE UNIVERSITY OF PARDUBICE
Series A
Faculty of Chemical Technology
10 (2004)

TRANSITION METAL-DOPED Sb_2Te_3 SINGLE CRYSTALS

Petr LOŠŤÁK[a1], Čestmír DRAŠAR[b] and Ctirad UHER[c]
[a]Department of General and Inorganic Chemistry, [b]Department of Physics,
The University of Pardubice, CZ–532 10 Pardubice,
[c]Department of Physics, University of Michigan,
Ann Arbor, Michigan 48109, USA

Received September 22, 2004

In this review paper we present and discuss results of extensive studies made on single crystals of the tetradymite-type compound Sb_2Te_3 doped with the transition metal elements. We focus on the transport and magnetic measurements made over the temperature range 2 – 300K and show that the $Sb_{2-x}Me_xTe_3$ (Me = Ti, Mn, V, and Cr) compounds reveal a variety of interesting physical properties. Among them is the existence of a long-range magnetic order that characterizes some of the compounds as novel diluted magnetic semiconductors.

Introduction

Antimony telluride Sb_2Te_3 belongs to the layered-type semiconductors with tetradymite structure (space group D_{3d}^5), which are used as materials for the

[1] To whom correspondence should be addressed.

construction of thermogenerators and solid-state coolers [1]. For the application of Sb_2Te_3 in these devices it is necessary to prepare a single or polycrystalline material with defined physical parameters (electrical and thermal conductivity, mobility of free current carriers, thermoelectric power) that can be modified by doping with suitable foreign atoms. Therefore, an investigation of the effect of various dopants on the physical properties of Sb_2Te_3 is interesting for both basic and applied research.

Despite considerable attention paid to the study of Sb_2Te_3 single crystals, only very little information is available on the influence of transition metal impurities on the properties of this material. The paper by J. Horak *et al.* [2] can be regarded as a pioneering work in this field, in which Mn-doped Sb_2Te_3 was studied. Based on reflectance spectra in infrared region it was concluded that Mn entering the crystal structure of Sb_2Te_3 raises the hole concentration. According to the authors, substitutional defects Mn'_{Sb} balanced with a hole account for this effect. Systematic research on crystals with the tetradymite structure doped with transition metals began in our group in 1995, when the study of optical properties of $Sb_{2-x}Ti_xTe_3$ system was published [3]. The measurements of transmittance and reflectance in infrared region show that Ti in Sb_2Te_3 depresses the hole concentration. This result is in accordance with the measurements of Hall coefficient and electrical resistivity published in Ref. [4], which is devoted to galvanomagnetic measurements. The measurements of Shubnikov–de Haas effect presented in that paper reveal that the conduction band of these crystals is split into two subbands. Correspondingly, the transport properties reflect the presence of both light and heavy holes. The anomalous feature in the Hall effect (the Hall coefficient increases in the temperature interval 77 – 300K) was explained by the presence of light and heavy holes.

The incorporation of Zr atoms into the crystal structure of Sb_2Te_3 results in a decrease in hole concentration as well. This fact is supported by the measurements of reflectance spectra, Hall coefficient, and electrical conductivity that were presented in [5].

In contrast to Ti and Zr, Cr atoms incorporated into the crystal structure of Sb_2Te_3 have practically no influence on the concentration of holes. In $Sb_{2-x}Cr_xTe_3$ single crystals, varying x from 0.0 to 0.07, we observed essentially no change in both the plasma resonance frequency and Hall coefficient. The falling electrical conductivity with the increasing content of Cr is related to a decrease in the mobility of holes [6].

In the present paper, we summarize interesting results of the cooperation between the teams from the Faculty of Chemical Technology, University of Pardubice and the Department of Physics, University of Michigan. The cooperation has been supported by the project "Novel Magnetic Semiconductors Based on Sb_2Te_3" and has focused on the characterization of single crystals of $Sb_{2-x}Me_xTe_3$ (Me = Ti, Mn, V, and Cr).

Experimental

Growth of Single Crystals and Preparation of Samples

The starting polycrystalline materials for growing the single crystals were prepared from the elements Sb, Ti, Mn, V, Cr, and Te of 5N purity.

The starting polycrystalline materials were prepared from the mixture of elements corresponding to the stoichiometry $Sb_{2-x}Me_xTe_3$ in silica ampoules evacuated to the pressure of 10^{-4} Pa. The synthesis was carried out in a horizontal furnace at 1073 K for 48 h.

The single crystals were grown using the Bridgman method. A conical quartz ampoule, containing the synthesized polycrystalline material, was placed in the upper (warmer) part of the Bridgman furnace, where it was annealed at 1003 K for 24 hours. Then it was lowered into a temperature gradient of 400 K $5\,cm^{-1}$ at a rate of 1.3 mm h^{-1}.

The obtained single crystals, 50 mm in length and 10 mm in diameter, could be easily cleaved. Their trigonal axis *c* was always perpendicular to the pulling direction so that the (0001) plane was parallel to the ampoule axis. The orientation of the cleavage faces was carried out using the Laue back-diffraction technique which confirmed that these faces were always (0001). To determine their physical properties, the samples of the dimensions of $10 \times 2 \times 2$ mm^3 were cut out from the middle part of the single crystals.

The concentration of transition metals in these samples was determined by atomic emission spectrometry (AES) and by electron microprobe analysis (EMPA).

Measurement of the Hall Coefficient, Electrical Resistivity, Seebeck Coefficient, Thermal Conductivity and Magnetic Susceptibility

The Hall effect and electrical resistivity were studied using a Linear Research ac bridge with 16 Hz excitation in a magnet cryostat capable of fields up to 5T.

Seebeck coefficient (thermopower) and thermal conductivity were determined using a longitudinal steady-state technique in a cryostat equipped with a radiation shield. Thermal gradients were measured with the aid of fine chromel-constantan differential thermocouples, and a miniature strain gauge served as a heater. For the Seebeck probes we used fine copper wires that have previously been calibrated, and their thermopower contribution subtracted from the measured sample thermopower.

Magnetic susceptibility and magnetization measurements were made in a Quantum Design superconducting quantum interference device magnetometer equipped with 5.5 T magnet.

Measurements of these parameters were made over the temperature range of 5 – 300K.

Results and Discussion

Properties of $Sb_{2-x}Ti_xTe_3$ Single Crystals

The single crystals of $Sb_{2-x}Ti_xTe_3$ (x = 0.00, 0.003, 0.009, 0.017) were characterized in paper [7]. Temperature dependences of the Hall coefficient $R_H(B//c)$, Seebeck coefficient $\alpha(\Delta T \perp c)$ and electrical resistivity $\rho_{\perp c}$ are presented in Figs 1 – 3. From the results obtained it can be seen that the incorporation of Ti atoms into the Sb_2Te_3 crystal structure results in an increase of all investigated parameters. The curves of $\alpha(\Delta T \perp c) = f(T)$ versus temperature of all the samples are similar with an exception of the sample with the highest Ti content (see Fig. 2); we assume that the anomalous temperature dependence of this sample is associated with a change in the scattering mechanism of free carriers. The data imply that Ti-doping of Sb_2Te_3 crystals leads to a decrease in the concentration of holes. This result agrees well with the reflectance and galvanomagnetic measurements reported in papers [3,4]. The observed decrease in the hole concentration due to Ti doping can be explained by the substitution of Sb atoms by Ti atoms.

In order to evaluate the charges on the point defects we use the bonding model of Krebs [8]. According to this model, Sb and Te atoms in the Sb_2Te_3 crystals are linked together by σ – bonds with the participation of 5p-orbitals of Sb and 5p-orbitals of Te. The electron configuration of the valence sphere of Sb is $5s^25p^3$ and each Sb atom donates three electrons to the σ – bonds. Therefore, each Ti atom at the Sb lattice position should also donate three electrons to these bonds. As the electron configuration of Ti is $[Ar]3d^24s^2$ we assume that when a Ti atom occupies the Sb lattice position, its two 3d and two 4s electrons are excited into the nearby situated 4p-orbitals; three of them take part in the formation of σ – bonds with Te atoms and the fourth electron is released into the conduction band. The substitutional defect, created in this way is, therefore, singly positively charged and designated as $Ti^{\bullet}_{Sb}$. Such incorporation of the Ti-atoms into the Sb_2Te_3 crystal lattice can be described by the following scheme

$$2Ti + 3Te \longrightarrow 2Ti^{\bullet}_{Sb} + 2e' \qquad (1)$$

The recombination of the above electrons with holes results in the observed decrease in the concentration of free current carriers. This scheme is in accordance

with the fact that all studied crystals are diamagnetic (Ti atoms are formally in the Ti^{4+} state).

The supposed incorporation of Ti atoms into the Sb-sublattice is supported by the results of X-ray diffraction [4] which confirm that an increasing content of Ti in Sb_2Te_3 leads to a decrease of the lattice parameters a and c and thus to a de-

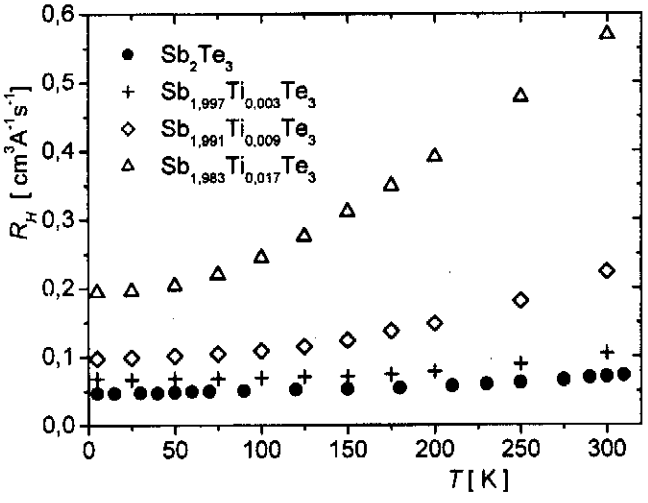

Fig. 1 Temperature dependence of the Hall coefficient $R_H(B//c)$ of Ti-doped Sb_2Te_3 single crystals

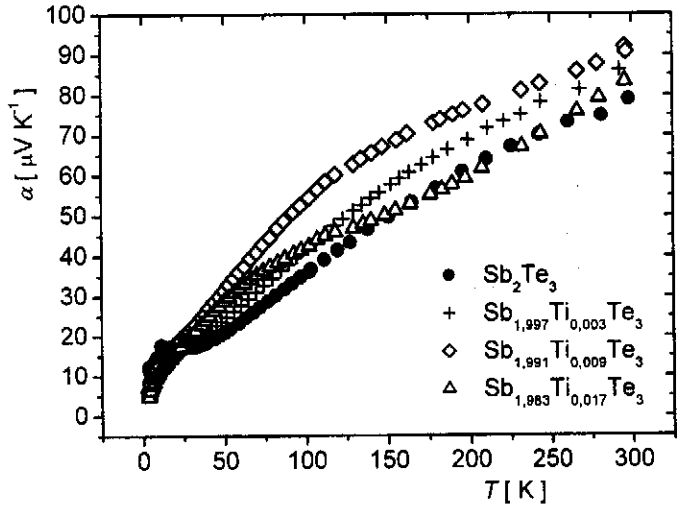

Fig. 2 Temperature dependence of the Seebeck coefficient $\alpha(\Delta T \perp c)$ of Ti-doped Sb_2Te_3 single crystals

crease in the unit cell volume. Noting that the crystal radius of Ti^{4+} (r(Ti) = 0.745 nm) is smaller than that of Sb^{3+} (r(Sb) = 0.900 nm), the decrea-

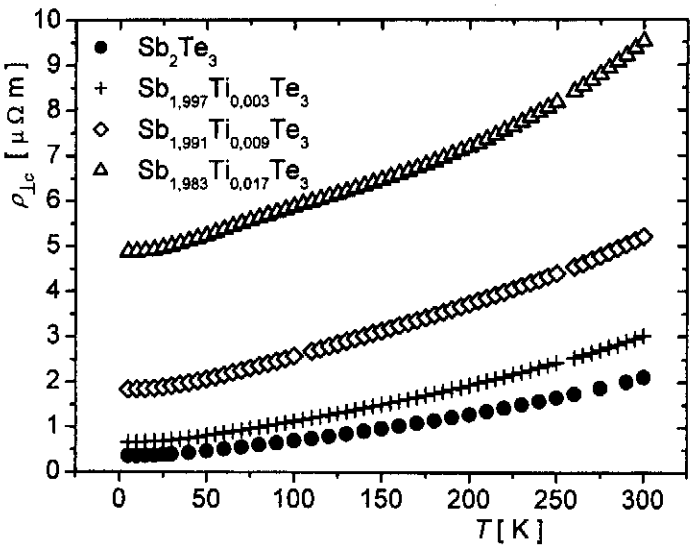

Fig. 3 Temperature dependence of the electrical resistivity $\rho_{\perp c}$ of Ti-doped Sb_2Te_3 single crystals

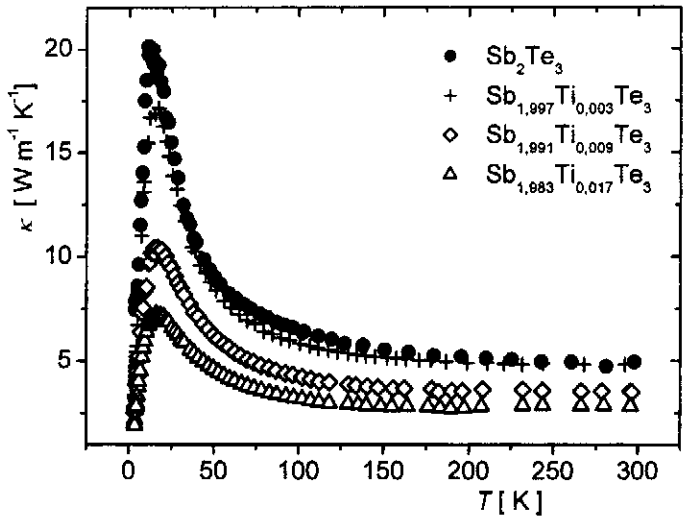

Fig. 4 Temperature dependence of the thermal conductivity κ of Ti-doped Sb_2Te_3 single crystals

se in the unit cell volume is expected.

The temperature dependence of the total thermal conductivity κ is given in Fig. 4. The values of κ for Sb_2Te_3 increase as temperature decreases and a peak develops at a temperature near 13 K. It is evident that the incorporation of Ti atoms into the Sb_2Te_3 crystal structure results in the suppression of the thermal conductivity at all temperatures.

Total thermal conductivity κ, in general, is the sum of two components; $\kappa = \kappa_L + \kappa_e$ where κ_e and κ_L are the electronic and lattice thermal conductivity contributions, respectively. The exact calculation of κ_e is complicated by the likely presence of two valence bands, the upper valence band (UVB) and the lower valence band (LVB) and hence of two kinds of holes. However, the two bands are not populated equally, the ratio of the LVB density of holes to that of the UVB hole density is equal to 390 [9]. In view of this large ratio, only the LVB holes are considered in further discussions.

The electronic component of the thermal conductivity κ_e was calculated from the experimental values of resistivity $\rho_{\perp c}$ using the Wiedemann–Franz relation $\kappa_e = LT/\rho_{\perp c}$, where L is the Lorenz number and T is the absolute temperature. In order to evaluate the effect of the scattering mechanism on the magnitude of κ_e, the value of the Lorenz number was determined from the general expression [10]

$$L = \left(\frac{k_B}{e}\right)^2 \left\{ \frac{(s + 7/2)F_{s+5/2}(\eta)}{(s + 3/2)F_{s+1/2}(\eta)} - \left[\frac{(s + 5/2)F_{s+3/2}(\eta)}{(s + 3/2)F_{s+1/2}(\eta)} \right]^2 \right\} \qquad (2)$$

where a value of $s = -1/2$ corresponds to the scattering on acoustic phonons, $s = 1/2$ to the scattering on optical phonons and $s = 3/2$ to the scattering on ionized impurities. The required values of the reduced Fermi level η were calculated from the experimental values of the Seebeck coefficient using the expression [10]

$$\alpha = \pm \frac{k_B}{e} \left(\frac{(s + 5/2)F_{s+3/2}(\eta)}{(s + 3/2)F_{s+1/2}(\eta)} - \eta \right) \qquad (3)$$

Fermi-integrals F_r in the expressions (2) and (3) are defined as

$$F_r(\eta) = \int_0^\infty \frac{x^r}{1 + \exp(x - \eta)} dx \qquad (4)$$

Since the temperature dependence of the Seebeck coefficient at temperatures below 50 K is influenced by phonon drag, the calculations were carried out only for temperatures above 50 K. One can compare the influence of several scattering mechanisms on the electronic thermal conductivity of Sb_2Te_3 in Fig. 5. We can

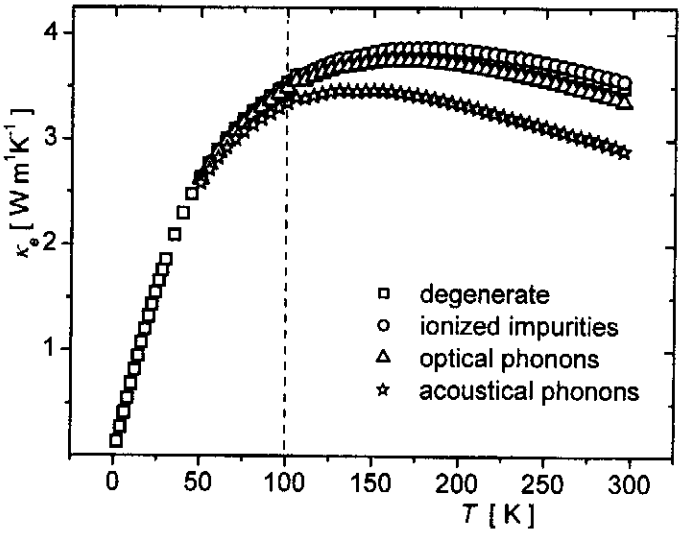

Fig. 5 Temperature dependence of the electronic part of thermal conductivity κ_e of Sb_2Te_3 single crystals assuming various scattering mechanisms

see hardly any difference between the result calculated with the constant value of the Lorenz number $L = L_0 = \frac{\pi^2}{3}\left(\frac{k_B}{e}\right)^2$ (degenerate system), and the results obtained assuming non-degenerate systems with a variety of scattering mechanisms acting below 100 K. So in the first approximation we use the Wiedemann–Franz relation $\kappa_e = L_0 T/\rho$ to calculate κ_e in this temperature region. Subtracting the electronic thermal conductivity contribution from the total measured thermal conductivity, we obtain the lattice thermal conductivity displayed in Fig. 6.

Temperature dependence of lattice thermal conductivity can be fitted within Debye approximation using the following expression [11]

$$\kappa_L(T) = \frac{k_B}{2\pi^2 v}\left(\frac{k_B T}{\hbar}\right)^3 \int_0^{\theta_D/T} \tau_C \frac{y^4 e^y}{(e^y - 1)^2} dy \qquad (5)$$

where k_B is the Boltzmann constant, $\hbar$ is the reduced Planck constant, y stands for the dimensionless parameter $y = \hbar\omega/k_B T$, ω is the phonon frequency, θ_D is Debye temperature, v is the velocity of sound, and τ_C is the phonon relaxation time. This relaxation time can be written in terms of the individual scattering times accounting for various scattering processes as follows

$$\tau_C^{-1} = \frac{v}{d} + A\omega^4 + B\omega^2 T \exp\left(-\frac{\theta_D}{3T}\right) + C\omega \qquad (6)$$

Here d is the crystal dimension (d = 2 mm for the smallest dimension of our crystals) and the coefficients A, B, and C are temperature independent fitting parameters. The terms in Eq. (6) stand for boundary, point-defect, three-phonon umklapp, and carrier-phonon scattering, respectively. The first three terms account for phonon scattering in dielectric crystals. The fourth term represents relaxation time for scattering of phonons by free carriers in a parabolic band as derived by

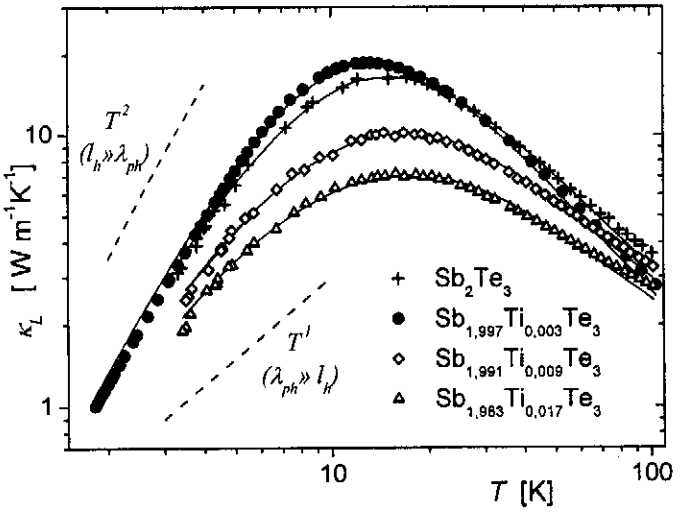

Fig. 6 Lattice thermal conductivity κ_L of Ti-doped Sb_2Te_3 single crystals. Solid lines are theoretical fits to Eqs (4) and (5)

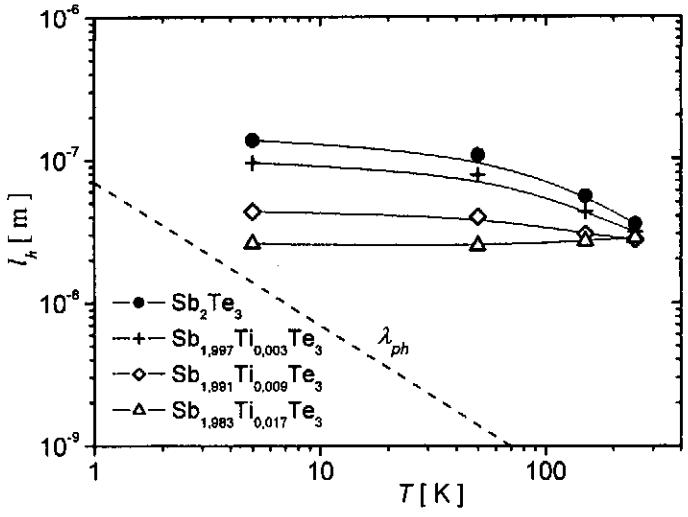

Fig. 7 Estimated hole mean free path l_h and phonon wavelength λ_{ph} as a function of temperature for Ti-doped Sb_2Te_3 single crystals

Ziman [12]. This term holds provided that $l_h \gg \lambda_{ph}$ where l_h is the mean free path of free carriers (holes) and λ_{ph} is the phonon wavelength. In Fig. 7, we show the comparison of λ_h and λ_{ph} estimated using the formal Drude analysis of the transport data and the dominant phonon method, respectively, for Ti-doped Sb_2Te_3. This illustrates that Eq. (6) is appropriate for Sb_2Te_3 while the doped samples may not fully satisfy the assumption, in which case the underlying theory might possibly break down [13]. Going from $l_h \gg \lambda_{ph}$ to $l_{ph} \gg \lambda_h, \tau_C$ becomes proportional to ω^2 rather than ω and consequently temperature dependence of κ_L becomes proportional to T rather than to T^2 in the respective temperature region (see Fig. 6). In spite of the fact that the phonon mean free path of the doped samples might not satisfy the condition $l_h \gg \lambda_{ph}$, leaving the last term out yields poor fits.

To make use of Eq. (5), one needs the Debye temperature θ_D. In fact, this temperature is strictly not a constant but is temperature dependent. While $\theta_D(T)$ is known for Bi_2Te_3 [14,15], the corresponding temperature dependence for Sb_2Te_3 is not available. We make here an assumption that, while different in magnitude, the $\theta_D(T)$ of both Bi_2Te_3 and Sb_2Te_3 are similar in their temperature dependence. Correspondingly, the temperature dependence of θ_D (Bi_2Te_3) was shifted to fit the value of $\theta_D(Sb_2Te_3)$ = 160 K at 80K and this dependence was fitted. The obtained polynomials

$$\theta_D(T = 2 - 8\,K) = 107.617 + 1.291T - 0.008T^2$$

$$\theta_D(T = 8 - 100\,K) = 91.258 + 3.188T - 0.064T^2 +$$
$$+ 5.895\times10^{-4}T^3 - 2.008\times10^{-6}T^4$$

were used for fitting of κ_L.

The sound velocity was estimated in [16] to be $v = 2900$ m s^{-1}. The results of the fit are summarized in Table I and in Fig. 6. Upon inspecting fitting parameters in Table I, it is evident that the point defect scattering parameter A controls the behaviour. It can be written as [17]

$$A = \frac{\Omega\Gamma}{4\pi v^3} \tag{7}$$

Table I Fitting parameters for theoretical analysis of lattice thermal conductivity of $Sb_{2-x}Ti_xTe_3$ single crystals as they refer to Eqs (5) and (6)

No.	x (actual)	A, 10^{-43} s^3	B, 10^{-18} s K^{-1}	C, 10^{-14}
1	0	9.65	27	0.82
2	0.003	17.6	20	0.85
3	0.009	55.5	17	1.03
4	0.017	113	16	1.11

where Ω is the unit cell volume (for Sb_2Te_3 $\Omega = 0.161$ nm^3), Γ is the scattering parameter which for a compound A_aB_b can be written as [18]

$$\Gamma(A_aB_b) = \frac{a}{a+b}\left(\frac{M_A}{M_m}\right)^2\Gamma(A) + \frac{b}{a+b}\left(\frac{M_B}{M_m}\right)^2\Gamma(B) \tag{8}$$

where M_m is the mean atomic mass of atoms composing the compound, $M_m = (aM_a + bM_b)/(a+b)$. $\Gamma(A, B)$ is the scattering parameter of the substitutional impurity at a respective site,

$$\Gamma(A, B) = \alpha(1-\alpha)\left[(\Delta M/M_{ave})^2 + \varepsilon(\Delta\delta/\delta_{ave})^2\right] \tag{9}$$

Here α ($\alpha = x/2$ in this case) is the relative concentration of impurity at a respective site, $\Delta M = M_i - M(A, B)$ is the atomic mass difference between the impurity and the atom normally associated with that lattice site, $\Delta\delta = \delta_i - \delta$ is the difference in radii between the impurity and the atom normally associated with that lattice site, M_{ave} and δ_{ave} are the weighted averages of mass and radius at that

lattice site, respectively, and ε is a phenomenological parameter. The first term of Eq. (9) accounts for mass fluctuation and the second term accounts for atomic radius fluctuations, i.e., elastic strain.

Table II Values of the parameter ε and the ratio R of $Sb_{2-x}Ti_xTe_3$ single crystals resulting from the analysis of parameter A, see text for details.

No.	x (actual)	ε	R
2	0.003	183	14.7
3	0.009	192	15.4
4	0.017	211	16.9

The exact radii of Sb and Ti in Sb_2Te_3 are unknown. The average distance between Sb and Te in the compound (0.311 nm) would rather support an ionic crystal picture ($r(Sb^{+3}) + r(Te^{-2})$ = 0.90 + 2.07 nm), as opposed to a covalent one (r(Sb) + r(Te) = 1.37 + 1.36 nm). To keep the things consistent, we use the ionic crystal values for all elements, including $r(Ti^{+4})$ = 0.745 nm [19,20].

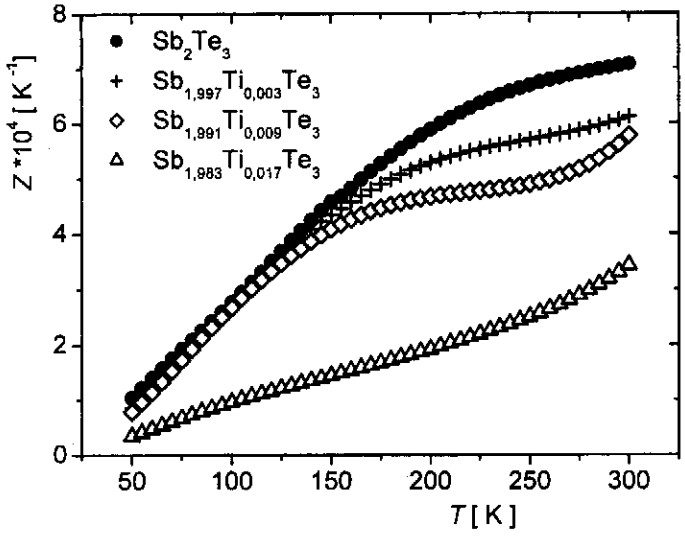

Fig. 8 Temperature dependence of the thermoelectric figure of merit Z of Ti-doped Sb_2Te_3 single crystals

The ε parameter and the ratio of strain field to mass fluctuation effects $R = \varepsilon(\Delta\delta/\delta_{ave})^2/(\Delta M/M_{ave})^2$ are summarized in Table II. The experimentally determined Ti content (AES-value) was used in the evaluation. The R values indicate that strain field plays a more important role than mass fluctuations.

The parameter B of the umklapp scattering term in Eq. (5) is written as [21]

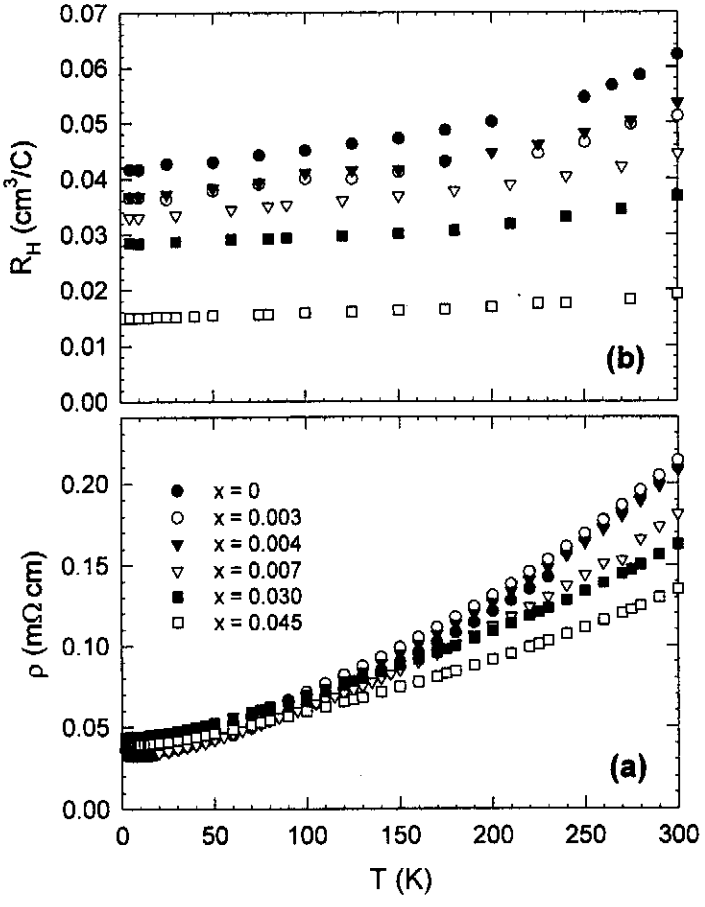

Fig. 9 (a) Electrical resistivity ρ and (b) Hall coefficient R_H data as a function of temperature for the series of $Sb_{2-x}Mn_xTe_3$ single crystals. Current is perpendicular to the *c*-axis, and magnetic field (for Hall effect) is parallel to the c-axis

$$B = \frac{n^{2/3}\hbar\gamma^2}{M\theta_D v^2} \tag{10}$$

This is a semiempirical formula where γ is the Grüneisen parameter, M is the average atomic weight, and n is the number of atoms in a molecule, here $n = 5$. We observe a small decrease of B with increasing Ti concentration, see Table II. A possible explanation is that titanium stiffens the lattice and increases the value of both θ_D and v. We note that the measurement of microhardness shows a roughly 20 % increase for the highest Ti concentration, which is within the measurement

accuracy.

The parameter C of carrier-phonon scattering can be written as [22]

$$C = \frac{(\xi m^*)^2}{2\pi\hbar^3\rho v} \tag{11}$$

where ξ is the deformation potential, m^* is the hole effective mass and ρ the density. We observe a small enhancement in the parameter C with increasing Ti concentration.

For the evaluation of the suitability of materials for thermoelectric applications the figure of merit $Z = \alpha^2/\kappa\rho_{\perp c}$ is usually applied. Temperature dependence of Z for Ti-doped Sb_2Te_3 crystals is given in Fig. 8. It is evident that doping Ti into Sb_2Te_3 crystals leads to a decrease in the value of the figure of merit.

Summarizing the discussion above we can draw the following conclusions:

1. Doping of Sb_2Te_3 crystals by Ti atoms results in a decrease in the concentration of holes. We assume that this effect is due to the incorporation of Ti atoms into the Sb sublattice and the formation of positively charged substitutional defects $Ti_{Sb}^{\bullet}$.
2. Lattice thermal conductivity was fitted well assuming that phonons scatter on boundaries, point defects, charge carriers, and other phonons within the Debye approximation. Incorporation of Ti atoms into the Sb_2Te_3 crystal lattice affects primarily point defect scattering.
3. Doping Sb_2Te_3 crystals by Ti atoms decreases the value of the figure of merit Z and, therefore, titanium is not an effective dopant for thermoelectric materials with the tetradymite type structure that are used for thermoelectric applications.

Properties of $Sb_{2-x}Mn_xTe_3$ Single Crystals

Magnetic and transport properties of the single crystals $Sb_{2-x}Mn_xTe_3$ ($x = 0 - 0.045$) were described in paper [23].

Electrical resistivity (current perpendicular to the c-axis) of Sb_2Te_3 is dominated by hole conduction and has a metallic temperature dependence characteristic of a degenerately doped semiconductor. The typical carrier concentration is $p \sim 1\times10^{20}$ cm^{-3} due to the presence of a large number of native antisite defects [25]. As shown in Fig. 9, the addition of manganese leads to a reduction of the resistivity and decrease in the Hall coefficient which is consistent with hole doping. At low x, these results agree with those of Horak *et al.* [2], while for values of $x > 0.01$, the doping rate is somewhat less than 1 hole per Mn atom.

A possible explanation is that the presence of Mn begins to affect the concentration of native defects [25–27], hence altering the number of background carriers.

Figure 10 displays the temperature dependence of the magnetic susceptibility for the $Sb_{2-x}Mn_xTe_3$ single crystals with the applied magnetic field (B = 1000 gauss) parallel to the c-axis. Antimony telluride is diamagnetic [28] and we measure a temperature independent value of $\chi = -3.8\times10^{-7}$ cm^3 g^{-1}. Samples containing Mn have a paramagnetic susceptibility. The data fit very nicely to a Curie–Weiss law of the form

$$\chi(T) = \frac{C}{T - \theta_{CW}} + \chi_0 \qquad (12)$$

where C is the Curie constant, θ_{CW} is the paramagnetic Curie temperature, and χ_0 is the temperature independent diamagnetic contribution of the host Sb_2Te_3 crystal. The fitting parameters are given in Table III. Calculations of the effective Bohr magneton number p_{eff} are made *via* the equation $C = Np_{eff}^2\mu_B^2/3k_B$ where N is the number of Mn ions (we take the EMPA value), μ_B is the Bohr magneton

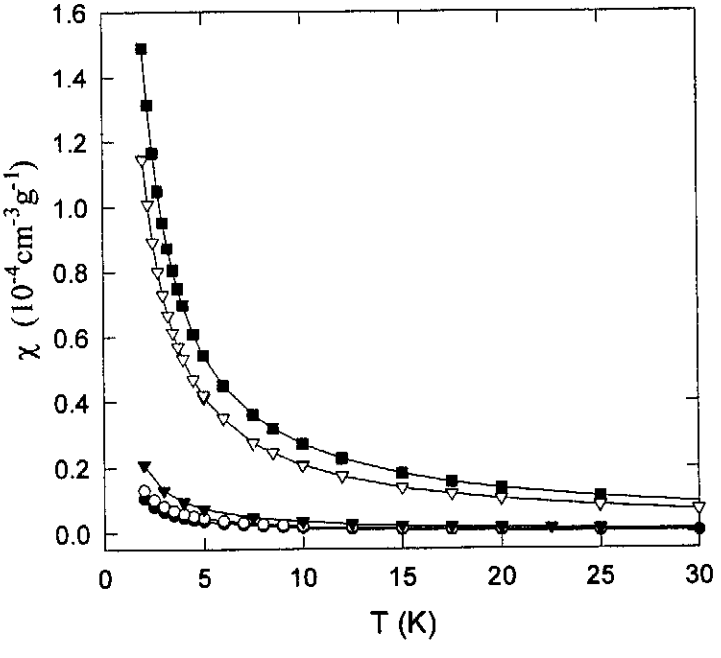

Fig. 10 Magnetic susceptibility χ versus temperature for the series of $Sb_{2-x}Mn_xTe_3$ single crystals. Symbol definitions are given in Fig. 9

number, and k_B is Boltzmann's constant. Values of $p_{eff} = g\sqrt{J(J+1)}$ are close to the value for high spin Mn^{2+} ($L = 0, S = 5/2$) of 5.92 μ_B taking the Landé g factor to be $g = 2$. With $\theta_{CW} \leq 0.3$ K, there is clearly no strong tendency toward ferromagnetic order among the spins. We also note that χ_0 values arising from the fitting analysis are very close to the expected value for Sb_2Te_3 for small x, and become less negative as x increases. This trend is consistent with a small (positive) Pauli paramagnetic contribution associated with the increased concentration of holes arising from the Mn substitutional ions. Low temperature magnetization data add further experimental evidence for the high spin Mn^{2+} state in $Sb_{2-x}Mn_xTe_3$. The data at several temperatures below 10 K for each composition were fit with a single Brillouin function with spin S and concentration of Mn x^* as free parameters. For all samples, $S = 5/2$ to within 5 % and x^* was close to the content x determined from EMPA. Figure 11a shows M versus B/T at several temperatures between 2 K and 10 K for $Sb_{1.997}Mn_{0.003}Te_3$ — the solid line is a fit to a Brillouin function with $S = 5/2$ and where only x^* is a free parameter (see Table III). For the other compositions with $x < 0.01$, the analysis yields very similar results. For larger x, the data at $T = 2$ K depart somewhat from the $S = 5/2$ curve, though the fit does not improve with a different value of S. The M versus B/T curve for $Sb_{1.955}Mn_{0.045}Te_3$ is shown in Fig. 11b. Perhaps correlation among spins becomes important for these high doping levels at temperatures near

Table III Results of the Curie-Weiss fitting for single crystals of $Sb_{2-x}Mn_xTe_3$. Also given are the concentration of manganese atoms as determined from EMPA (x) and from fitting to a Brillouin function assuming $S = 5/2$ (x^*). Effective Bohr magneton numbers calculated using the Mn content from EPMA (p_{eff}) and from the Brillouin analysis (p_{eff}^*) are included

x (from EMPA)	C $cm^3\,g^{-1}\,K^{-1}$	θ_{CW} K	χ_0 $cm^3\,g^{-1}$	p_{eff} μ_B/Mn ($g = 2$, using x)	x^* (from M vs. B)	p_{eff}^* μ_B/Mn ($g = 2$, using x^*)
0.003 ± 0.0008	1.83×10^{-5}	0.3	-3.50×10^{-7}	5.53	0.0027	5.83
0.004 ± 0.0007	2.28×10^{-5}	0.3	-3.38×10^{-7}	5.34	0.0034	5.8
0.007 ± 0.001	3.60×10^{-5}	0.3	-2.94×10^{-7}	5.07	0.0054	5.78
0.030 ± 0.002	2.00×10^{-4}	0.26	-1.95×10^{-8}	5.77	0.0295	5.82
0.045 ± 0.002	2.61×10^{-4}	0.25	9.57×10^{-8}	5.39	0.038	5.87

and below 2 K. Recalculated values of the effective Bohr magneton number p_{eff}^* using x^* rather than x are presented in Table III for comparison. For all samples p_{eff} is even closer to the value of 5.92 μ_B per Mn expected for the $S = 5/2$ state than values of p_{eff} calculated from x.

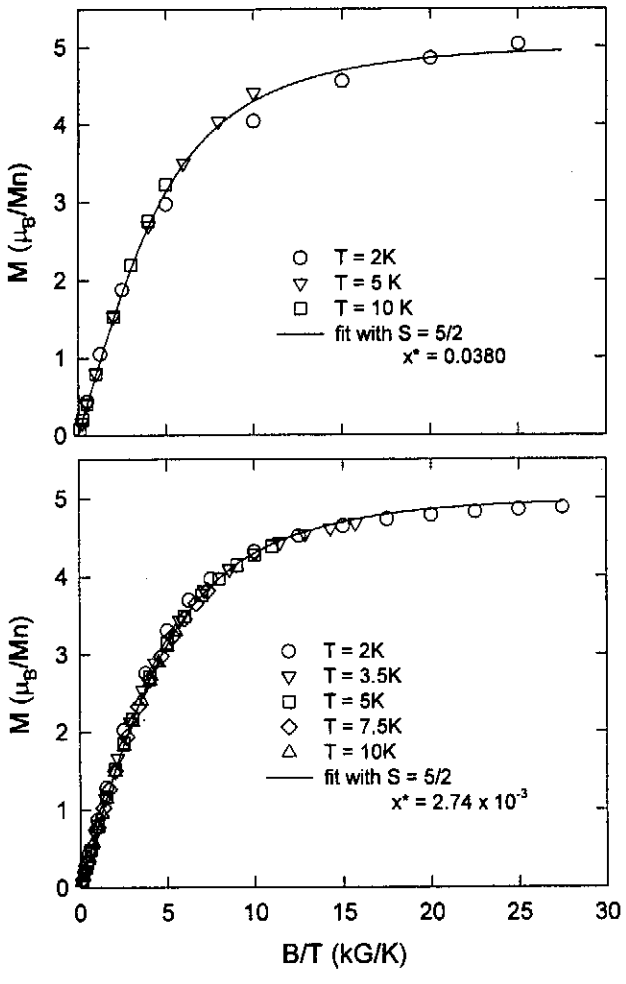

Fig. 11 Magnetization curves for single crystals of (a) $Sb_{1.997}Mn_{0.003}Te_3$ and (b) $Sb_{1.955}Mn_{0.045}Te_3$ at several temperatures. Magnetic field B is oriented parallel to the c-axis. Solid lines are fits of the data to a Brillouin function assuming $S = 5/2$ where the manganese content x^* is a fitting parameter

With strong evidence for the predominance of the Mn^{2+} state, we can postulate the location of the substitutional ions in the lattice. In pure Sb_2Te_3, each Sb atom ($5s^25p^3$) supplies three electrons and each Te ($5s^25p^4$) gains two in forming the σ bonds of the diamagnetic solid. Manganese ($3d^54s^2$) apparently provides its two s-electrons to bonding. Were it situated on Te sites, this atom would be deficient two electrons thereby creating two holes in the valence band, contrary to the Hall data indicating an approximate doping rate of one hole per Mn. Rather, a picture of Mn substituting for Sb, with the $4s^2$ electrons of Mn

replacing the $5p^3$ electrons of Sb, would result in the observed doping rate of one hole per Mn. Our interpretation is consistent with that by Horák *et al.* [2], though they calculate 1.8 μ_B per Mn from magnetic susceptibility data, which implies a S = 1/2 state. According to Horák *et al.* [2] this low spin arrangement can be understood by considering that the d-orbitals of the Mn atom will be split by the octahedral field of the six Te atoms into a triply degenerate lower t_{2g} orbital and a doubly degenerate e_g orbital. Provided the crystal field splitting is large enough, the five d-electrons will fill only the t_{2g} orbital with two pairs of spin-paired electrons and a single unpaired electron. In contrast, our data provide strong evidence for the high spin $S = 5/2 (t_{2g})^3(e_g)^2$ configuration implying that the crystal field splitting is too small to realize the $(t_{2g})^5(e_g)^0$ configuration. This discrepancy is not understood at this time. However, we note that Mn^{2+} is commonly observed to reside in the high spin state in diluted magnetic semiconductor (DMS) structures [29]. In particular, Mn has S = 5/2 in $Pb_{1-x}Mn_xTe$ [30], an environment where the Mn is also octahedrally coordinated by six Te atoms.

In conclusion, we find that single crystals of $Sb_{2-x}Mn_xTe_3$ for x = 0.003 - 0.045 are paramagnetic down to 2 K. Both low temperature magnetization data and low field magnetic susceptibility data up to room temperature indicate 5 unpaired spins per manganese atom. Together with Hall data that reveal an approximate doping rate of one hole per Mn atom, these results show that Mn takes the divalent, $S = 5/2 (3d^5)$ electronic configuration.

Ferromagnetic Ordering in $Sb_{2-x}V_xTe_3$ Single Crystals

We reported on a novel diluted magnetic semiconductor based on the Sb_2Te_3 tetradymite structure doped with very low concentration of vanadium (x = 0.01 - 0.03 for stoichiometry $Sb_{2-x}V_xTe_3$) in the papers [31,32]. The anomalous transport behaviour and robust magnetic hysteresis loops observed in magnetotransport and magnetic measurements were experimental manifestations of the ferromagnetic state in these materials. Curie temperature T_C of at least 22 K was observed for $Sb_{1.97}V_{0.03}Te_3$.

Magnetic susceptibility χ versus temperature obtained by cooling in a field of 1 kG oriented parallel to the c-axis of the samples is shown in Fig. 12. A value of $\chi = -3.8\times10^{-7}$ emu g^{-1}, roughly independent of temperature, was found for Sb_2Te_3 confirming the diamagnetic nature of pure $A_2^{V}B_3^{VI}$ tetradymite semiconductors. The transition to the ferromagnetic state for the samples containing vanadium is very clear as χ becomes positive and very large below T_C. Above the magnetic transition temperature, the magnetic susceptibility is well described by a Curie–Weiss law. The fits to the data using Eq. (12) are shown in the inset of Fig. 12 and the fitting parameters are given in Table IV. For a given

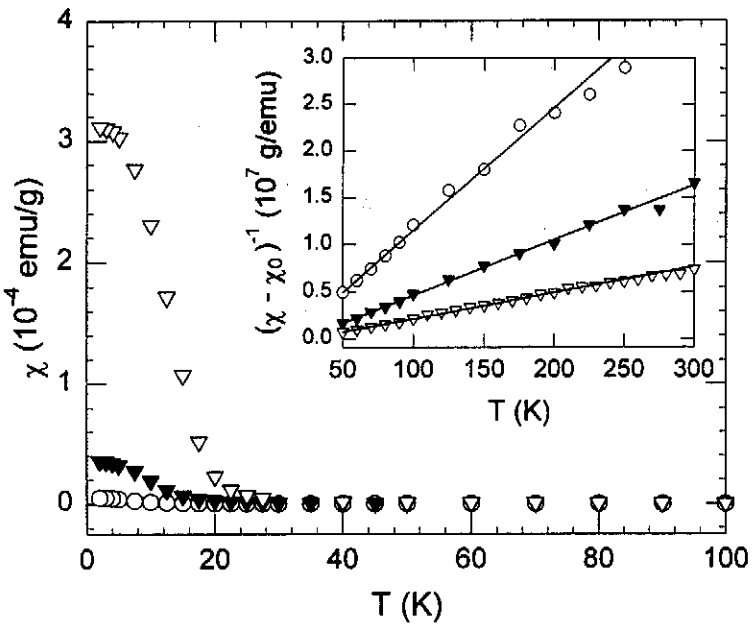

Fig. 12 Magnetic susceptibility χ versus temperaure for $Sb_{2-x}V_xTe_3$ with x = 0.01 (open circles), x = 0.02 (filled triangles), and x = 0.03 (open triangles). The inset shows the experimental data together with a fit to a Curie–Weiss law [Eq.(12)]. The fitting parameters are given in Table IV

Table IV Parameters from the fit of the magnetic susceptibility data to the Curie–Weiss law (Eq. (12)) for $Sb_{2-x}V_xTe_3$ crystals. Included are the ferromagnetic transition temperature T_C estimated from the magnetization data, the effective Bohr magneton number per vanadium atom $p_{eff}(\chi)$ obtained from the Curie constant, and the effective Bohr magneton number per vanadium atom $p_{eff}(M)$ obtained from the saturation value of the magnetization at 2 K

x	C emu K g^{-1}	χ_0 emu g^{-1}	θ_{CW} K	T_C K	$p_{eff}(\chi)$	$p_{eff}(M)$
0.01	7.61×10^{-6}	-4.03×10^{-7}	12.5	14	1.9	1.5
0.02	1.70×10^{-5}	-4.21×10^{-7}	21.2	18	2.1	1.8
0.03	3.60×10^{-5}	4.72×10^{-7}	23.4	22	2.5	2.1

concentration of vanadium in each sample, the magnetic state of the ions can be inferred from the Curie constant using the equation $C = N_V\mu_B^2 p_{eff}^2/3k_B$. Here, N_V is the concentration of vanadium atoms, μ_B is the Bohr magneton, p_{eff} is the effective Bohr magneton number given by $g[S(S+1)]^{1/2}$ with the Landé g factor (g = 2) and the spin S. We are assuming complete quenching of the orbital angular momentum, which is the usual case for transition metal ions. We note that

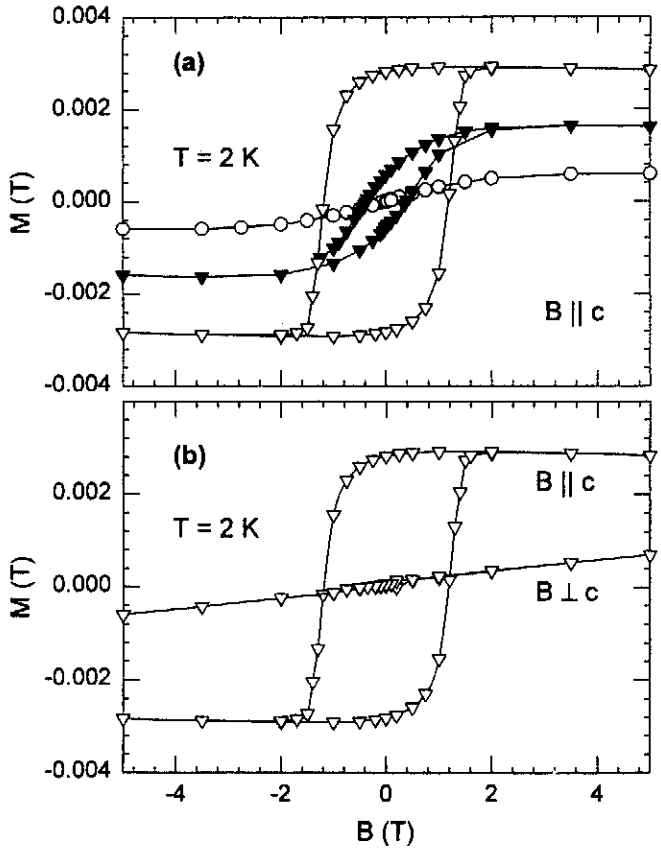

Fig. 13 Field dependence of the magnetization M for $Sb_{2-x}V_xTe_3$ with x = 0.01 (open circles), x = 0.02 (filled triangles), and x = 0.03 (open triangles). In (a), the field is aligned parallel to the c-axis. In (b), data for x = 0.03 are shown for the field aligned both parallel and perpendicular to the c-axis indicating that the c-axis is the easy axis for magnetization

the values of p_{eff} increase from 1.9 to 2.6 as x increases from 0.01 to 0.03. This might indicate an evolution to a predominantly 3+ valence state of vanadium (expected spin only value of p_{eff} = 2.83). We caution, however, that the very low concentrations of vanadium in these samples leads to uncertainty in the determination of x and hence p_{eff}. Detailed electron spectroscopy studies would shed more light on this issue.

The magnetization as a function of magnetic field for $Sb_{2-x}V_xTe_3$ is shown in Fig. 13. The wide hysteresis loops observed when the field is oriented parallel to the c-axis (Fig. 13a) are an unambiguous signature of ferromagnetic ordering in these samples. Although not obvious from the plot, the x = 0.01 sample shows hysteresis with a small coercive field of approximately 250 G. Such smooth

hysteresis loops (no apparent discontinuities) are suggestive of coherent rotation [33] of spins in this system. Another estimate of the spin of the vanadium ions can be obtained using the equation $M_s = N_V g \mu_B S$ and the results are given in Table IV. Again we can see a similar trend in the effective Bohr magneton numbers as the vanadium content increases. When the magnetic field is applied perpendicular to the *c*-axis as shown in Fig. 13b, practically no hysteresis is detected, indicating that the easy axis for magnetization is parallel to the *c*-axis. This may reflect the anisotropic structure of the tetradymite semiconductors.

Anomalies in the low-temperature transport properties of $Sb_{2-x}V_xTe_3$ provided additional evidence of the developing long-range magnetic order. Temperature dependence of the in-plane ($I \perp c$) resistivity ρ and Hall coefficient R_H are shown in Figs. 14 and 15, respectively. Resistivity of the pure Sb_2Te_3 sample increases linearly with temperature over the entire temperature range indicating degenerate Fermi gas carrier transport. The Hall coefficient R_H is positive with the modest temperature dependence for Sb_2Te_3. The room-temperature carrier (hole) concentration for Sb_2Te_3 is 1.0×10^{20} cm^{-3} due to native defects, typical for this compound. Upon addition of vanadium, the resistivity increases but remains metallic, while the values of the carrier concentration change very little. The room-temperature properties are summarized in Table VI. Error in the Hall hole concentrations is approximately 5 %.

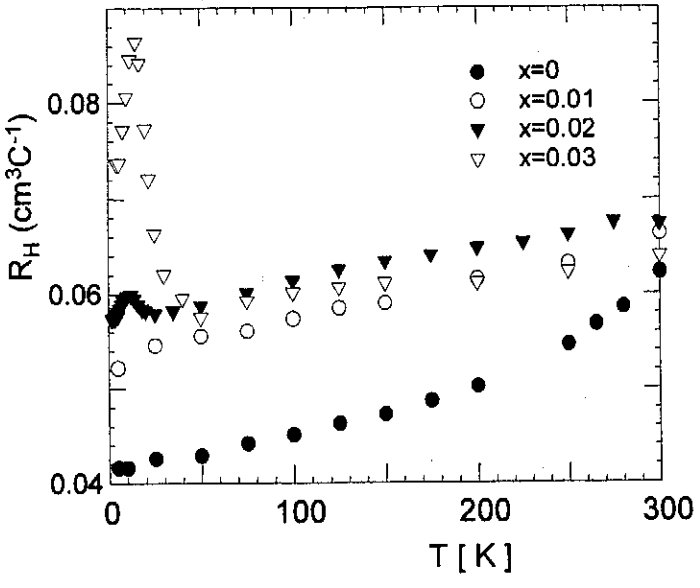

Fig. 14 Temperature dependence of Hall coefficient R_H determined in a field of 10 kG for $Sb_{2-x}V_xTe_3$

Table V Values of the hole concentration, p, resistivity, ρ, and Hall mobility, μ_H, determined at room temperature for $Sb_{2-x}V_xTe_3$ crystals

x	p cm^{-3}	ρ $\mu\Omega$ m	μ_H $cm^2 V^{-1} s^{-1}$
0	1.0×10^{20}	2.1	297
0.01	9.4×10^{19}	4.4	152
0.02	9.3×10^{19}	6.6	103
0.03	9.8×10^{19}	9.8	65

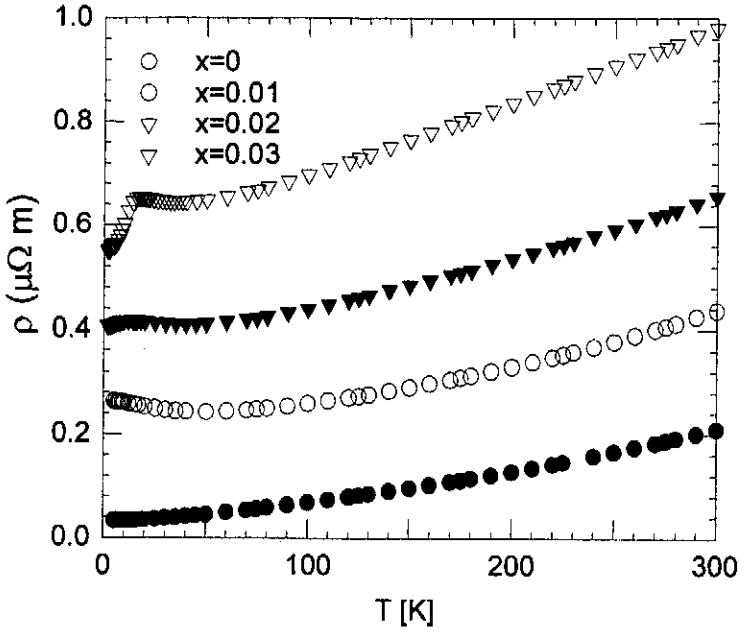

Fig. 15 Temperature dependence of in-plane resistivity ρ for $Sb_{2-x}V_xTe_3$

Below 30 K the presence of vanadium leads to a peak in both ρ and R_H that moves to higher temperature as the vanadium content increases. Magnetic semiconductors commonly exhibit a maximum in ρ near their Curie temperature T_C [34]. This critical behavior arises due to scattering of carriers by magnetic spin fluctuations *via* the exchange interaction (for more details see Ref. [32]).

The peak in R_H can be understood by considering the anomalous Hall effect [35], in which the Hall resistivity ρ_H is expressed as

$$\rho_H = R_0 B + R_s M \tag{13}$$

where R_0 is the ordinary Hall coefficient, R_s the anomalous Hall coefficient, and

M the magnetization of the samples. For temperatures above T_C, ρ_H is linear in magnetic field up to B = 50 kG with zero intercept implying that the second term in Eq. (13) is insignificant in this temperature range. Below T_C, the transition to the ferromagnetic phase results in a large M and thus the second term becomes significant. The maximum in R_H seen in Fig. 15 results from a peak in R_s that occurs at a temperature close to T_C in ferromagnetic materials [35].

In summary, a diluted magnetic semiconductor based on the vanadium-doped Sb_2Te_3 was discovered. The sample with composition $Sb_{1.97}V_{0.03}Te_3$ had a hole concentration of 9.8×10^{19} cm^{-3} and a Curie temperature of at least 22 K. Magnetization studies revealed that the easy axis for magnetization lies along the trigonal crystallographic axis (the c-axis).

We note, that a study of the heat transport in single crystals of $Sb_{2-x}V_xTe_3$ was presented in paper [16]. Thermopower and thermal conductivity were measured from 1.5 K to 300 K. The thermopower was positive for all the samples investigated and had a modest dependence on vanadium content. At low temperatures, the lattice thermal conductivity displayed an approximate T^2 dependence and the data up to 100 K can be fitted well assuming that phonons scatter on boundaries, point defects, charge carriers, and other phonons. Theoretical analysis reveals that the overriding effect of vanadium impurity is the formation of point defects that suppress heat transport *via* both mass and elastic strain fluctuations.

Ferromagnetic Ordering in $Sb_{2-x}Cr_xTe_3$ Single Crystals

Transport and magnetic measurements on $Sb_{2-x}Cr_xTe_3$ single crystals that are described in Ref. [36] give the evidence that the structure undergoes a ferromagnetic transition at low temperatures. The Curie temperature is proportional to x (for $x > 0.014$), attaining a maximum value of 20 K for $x = 0.095$.

Figure 16 displays the temperature dependence of the electrical resistivity ρ and Hall coefficient R_H of the $Sb_{2-x}Cr_xTe_3$ single crystals. As the concentration of Cr in the lattice increases, the electrical resistance increases smoothly over the entire temperature range. The Hall coefficient has a non-monotonic behavior as a function of x, with R_H first increasing by about 40 % followed by a shallow decrease with increasing x. The inset in Fig. 16a shows the room temperature Hall concentration as a function of Cr content. These data suggest that the concentration of holes is not strongly affected by the presence of Cr. One possible explanation for the initial suppression of the Hall concentration (see inset in Fig. 16a) is that the presence of low concentrations of Cr affects the concentration of native defects [25,27]. The transport data are in agreement with Ref. [6], in which temperature range above 100 K was explored.

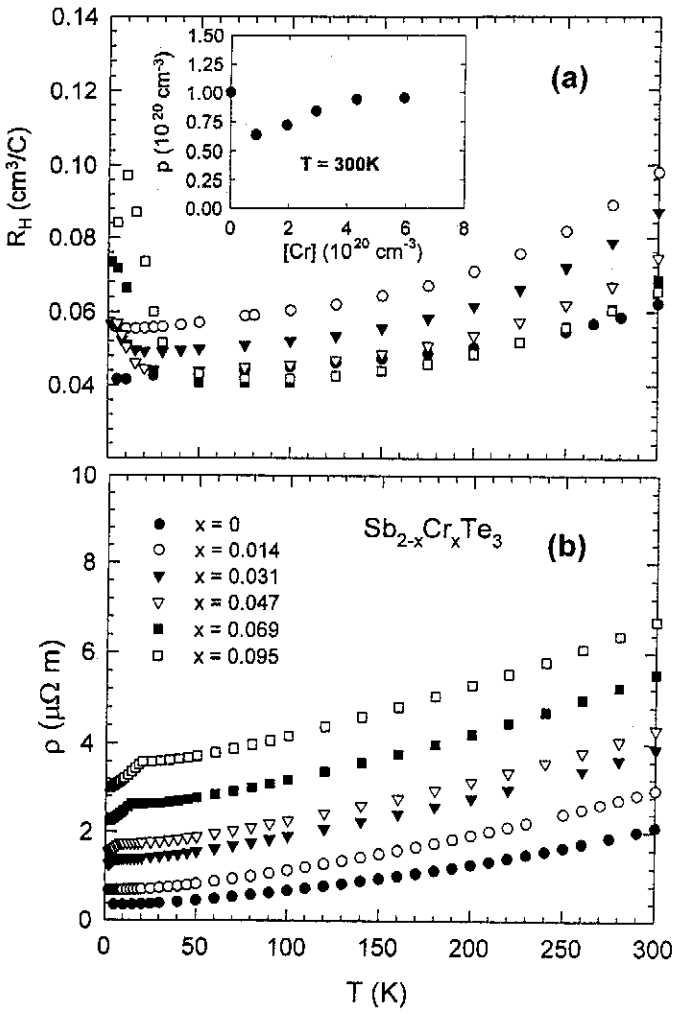

Fig. 16 (a) In-plane electrical resistivity ρ and (b) Hall coefficient R_H as a function of temperature for $Sb_{2-x}Cr_xTe_3$ single crystals. Current is perpendicular to the *c*-axis. The Hall concentration at room temperature is shown in the inset

At low temperatures, the resistivity data for samples with Cr content greater than $x = 0.014$ display a maximum. Hall coefficient data taken at low temperatures also reveal an upturn that occurs at the same temperature at which the ρ data display a peak. This behaviour is caused by a strong anomalous component in the transverse resistivity that is related to ferromagnetic ordering setting in at low temperatures. The temperature at which these transport anomalies are observed corresponds to the Curie temperature obtained from magnetic measurements. We note that similar features have been observed in other diluted

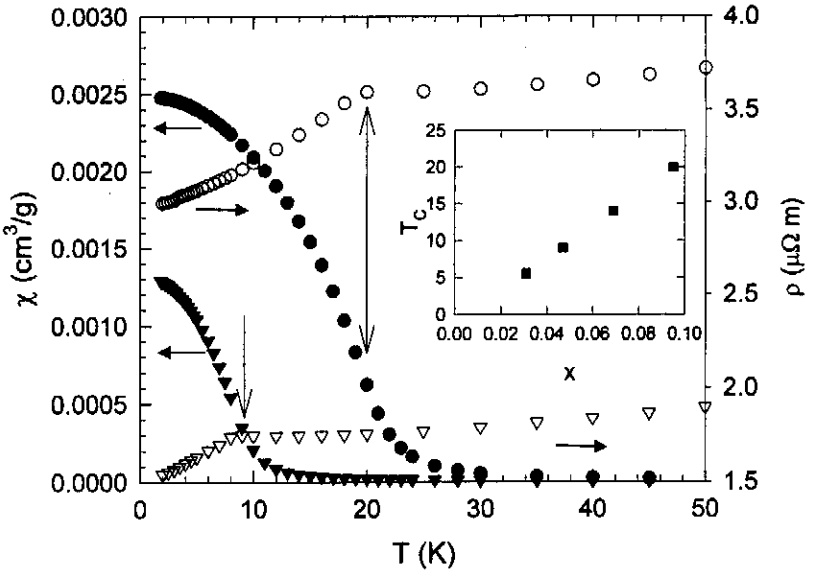

Fig. 17 Temperature dependence of the magnetic susceptibility χ (cooling in B = 1000 G parallel to c-axis) and in-plane resistivity ρ for $Sb_{2-x}Cr_xTe_3$ single crystals with x = 0.047 (triangles) and x = 0.095 (circles). The inset shows the Curie temperature T_C as a function of x

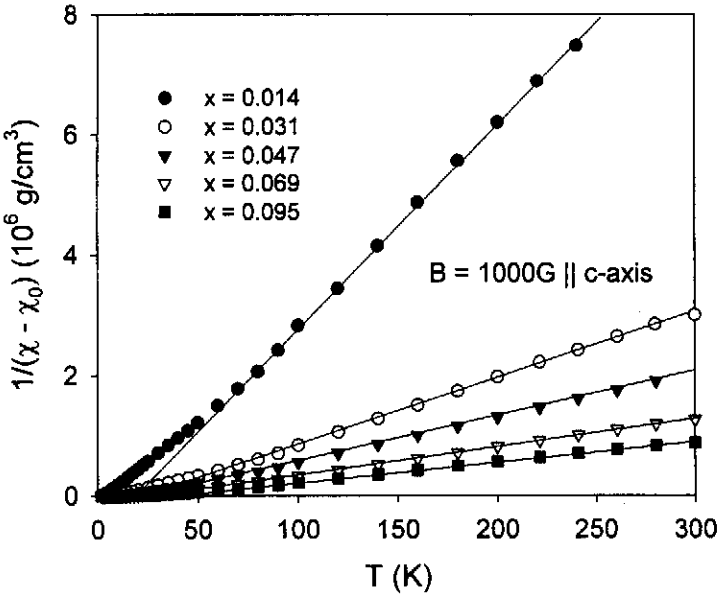

Fig. 18 Inverse magnetic susceptibility versus temperature for $Sb_{2-x}Cr_xTe_3$ single crystals

magnetic semiconductors such as $Ga_{1-x}Mn_xAs$ [37], $In_{1-x}Mn_xSb$ [38].

Representative magnetization data for temperatures below 50 K, together with the corresponding zero-field resistivities, are shown in Fig. 17 for $Sb_{2-x}Cr_xTe_3$ with x = 0.047 and x = 0.095. The magnetization data were collected while cooling in a field of 0.1 T oriented parallel to the c-axis. The magnetic susceptibility χ displays a sharp rise at T_C, as expected from the onset of long-range ferromagnetic order. One can see that the resistivity peak T_ρ occurs at the same temperature as the point of inflection in $\chi(T)$, and this correspondence was used to determine the Curie temperature. The inset in Fig. 17 shows a plot of T_C as a function of chromium content, x. The linear dependence of T_C on x is expected for diluted magnetic semiconductors. The lowest temperature of 1.8 K was not low enough to determine T_C for two specimens with x = 0.014, and these samples did not display measurable hysteresis in the M(H) curves above 1.8 K.

Above T_C, the magnetic susceptibility χ has paramagnetic behaviour for Cr-doped specimens. For temperatures above 100 K, the $Sb_{2-x}Cr_xTe_3$ data fit well to a Curie–Weiss law (12). Figure 18 displays the temperature dependence of the quantity $(\chi - \chi_0)^{-1}$. The fitting parameters are given in Table VI. It is evident that the values of spins per Cr atom S/Cr are close to 3/2, which corresponds to the $3d^3$ configuration of chromium atoms in the Cr^{3+} state.

The appearance of a ferromagnetic state in $Sb_{2-x}Cr_xTe_3$ was unambiguously confirmed by distinct hysteresis loops in the magnetization as well as Hall effect. Figure 19 shows the Hall resistivity and magnetization loops for a sample with x = 0.095 at T = 5 K. The observation of the anomalous Hall effect including clear hysteresis loops establishes Cr-doped Sb_2Te_3 as a homogeneous, ferromagnetic diluted magnetic semiconductor. Hysteresis in both magnetization

Table VI Summary of Curie-Weiss fitting of magnetic susceptibility data over the temperature range 100 K to 300 K for single crystal of $Sb_{2-x}Cr_xTe_3$

x (EMPA)	C $cm^3\,K\,g^{-1}$	θ_{CW} K	χ_0 $cm^3\,g^{-1}$	p_{eff}/Cr	S/Cr
0.014 ± 0.001	3.01×10^{-5}	15.16	-3.14×10^{-7}	3.28	1.22
0.031 ± 0.014	8.94×10^{-5}	24.95	-1.91×10^{-7}	3.8	1.47
0.047 ± 0.003	1.35×10^{-4}	24.72	1.83×10^{-8}	3.79	1.46
0.069 ± 0.001	2.10×10^{-4}	30.69	-1.79×10^{-7}	3.9	1.51
0.095 ± 0.001	2.91×10^{-4}	37.11	-2.36×10^{-7}	3.92	1.52

and anomalous Hall effect was observed in all the samples with $x \geq 0.031$.

One of the unusual characteristics of diluted magnetic semiconductors with the tetradymite structure is anisotropy in the magnetic properties. The easy axis for magnetization in these compounds is parallel to the c-axis and, for $Sb_{2-x}Cr_xTe_3$ crystals, the anisotropy field (field where the magnetization parallel to the c-axis

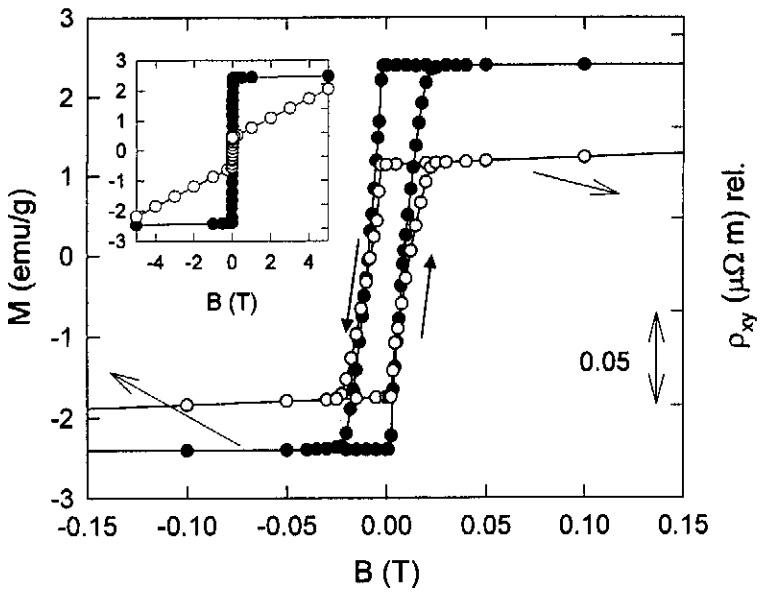

Fig. 19 Hysteresis loops in magnetization M and Hall resistivity ρ_{xy} at a temperature of 5 K for a single crystal of $Sb_{1.905}Cr_{0.095}Te_3$. Magnetic field is oriented parallel to the c-axis

is equal to that perpendicular to the c-axis) is much greater than 5T [32]. A comparison of hysteresis loops of the magnetization at 2 K for $Sb_{2-x}V_xTe_3$ with x = 0.03 and $Sb_{2-x}Cr_xTe_3$ with x = 0.095 is shown in Fig. 20. The coercive field H_C is much greater for the vanadium-doped Sb_2Te_3 with H_C = 1.2 T than for the Cr-doped Sb_2Te_3 with H_C = 0.015 T. Furthermore, while both compounds show an easy axis along the c-axis, the Cr-doped compounds reach a fully saturated state at a much lower field for B perpendicular to the c-axis (about 2T) as compared to the equally oriented V-doped Sb_2Te_3 compounds where B » 5 T. This fact indicates that the mechanism of magnetic order and domain structure may be somewhat different in the two materials.

In summary, single crystals of $Sb_{2-x}Cr_xTe_3$ for $x \geq 0.031$ are ferromagnetic, with Curie temperatures that depend linearly on the content of chromium. The maximum value of T_C is 20 K for x = 0.095. The ferromagnetic state was confirmed by hysteresis in both magnetization and Hall effect measurements. Magnetization studies reveal that the easy axis of magnetization is parallel to the c-axis of the structure. Magnetic as well as transport data indicate that Cr takes the 3+ ($3d^3$) valence state, substitutes for antimony in the host lattice structure, and does not significantly affect the background hole concentration.

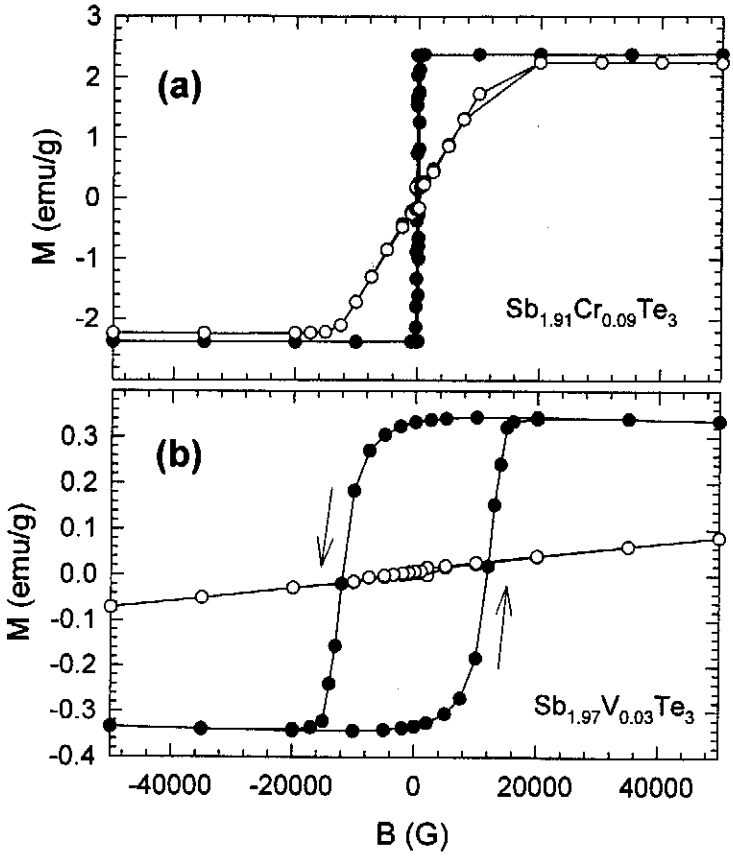

Fig. 20 Comparison of hysteresis in magnetization with applied magnetic field both parallel and perpendicular to the *c*-axis for Cr-doped Sb_2Te_3 and V-doped Sb_2Te_3 taken at 2 K

Conclusion

The study of transport and magnetic properties of Sb_2Te_3 single crystals doped with trasition metals such as V and Cr leads to a striking finding that single crystals $Sb_{2-x}V_xTe_3$ and $Sb_{2-x}Cr_xTe_3$ show ferromagnetic ordering at low temperatures. These materials represent a new type of diluted magnetic semiconductors (DMS). A significant feature of DMS's based on Sb_2Te_3 is the strong anisotropy of magnetic properties, which is related to their layered crystal structure. Besides these two systems, ferromagnetic monocrystals of $Bi_{2-x}Fe_xTe_3$ that belong to the same family of compounds were described in the literature [39].

Diluted magnetic semiconductors attract worldwide attention due to their possible applications as spintronic devices [40]. Recent research activity has

focused mainly on DMS materials based on $A^{II}B^{VI}$ (e.g., CdTe, ZnTe, ZnO), $A^{III}B^{VI}$ (e.g., GaAs, GaN), and $A^{IV}B^{VI}$ (e.g., PbTe, SnTe) compounds [41–45]. Practical applications require the existence of a robust ferromagnetic order at temperatures above 300 K. Accordingly, the challenge we face is to find a means by which we can raise the Curie temperature of the tetradymite-type DMS's above an ambient temperature. Possible approaches include increasing the carrier density, increasing the ferromagnetic coupling, and identifying more efficient transition metals that would stimulate magnetic ordering. We look forward to tacking these research challenges.

Acknowledgements

This work has been supported by the National Science Foundation International Grant No. 0201114 and by the Ministry of Education, Youth and Sports of the Czech Republic under the project KONTAKT ME 513.

References

[1] Nolas G. S.Sharp J., Goldsmid H.J.: *Thermoelectrics, Basic Principles and New Materials Developments*, p. 111, Springer, Berlin, Heidelberg, 2001.
[2] Horák J., Matyáš M., Tichý L.: Phys. Stat. Sol. (a) **27**, 621 (1975).
[3] Drašar Č., Lošťák P., Navrátil J., Černohorský T., Mach V.: Phys. Stat. Sol. (b) **191**, 523 (1995).
[4] Kulbachinskii V. A., Miura N., Nakagawa H., Drašar Č., Lošťák P.: J. Phys.: Condens. Mater. **11**, 5273 (1999).
[5] Lošťák P., Drašar Č., Klichová I., Navrátil J., Vlček M.: Cryst. Res. Technol. **32**, 369 (1997).
[6] Lošťák P., Drašar Č., Navrátil J., Beneš L.: Cryst. Res. Technol. **31**, 403 (1996).
[7] Drašar Č., Steihart M., Švanda P., Lošťák P., Shin H.-K., Dyck J. S.,, C. Uher C.: J. Solid State Chem., submitted.
[8] Krebs H.: *Grundzüge der anorganischen Kristallchemie*, p. 239, F. Enke, Stuttgart, 1968.
[9] Kulbachinskii V.A., Dashevskii Z.M., Inoue M., Sasaki M., Negishi H., Gao W.X., Lošťák P., Horák J., de Visser A.: Phys. Rev. B **52**, 10915 (1995).
[10] Oskotskii V.S., Smirnov I.A.: *Defekty v Kristallakh i Teploprovodnost*, p. 25, Ind. Nauka, Leningrad, 1972.
[11] Callaway J.: Phys. Rev. **113**, 1046 (1959).
[12] Ziman J.M.: *Electrons and Phonons*, pp.326 - 333 , Clarendon, Oxford, UK, 1960.

[13] Pippard A.B.: Philos. Mag. **46**, 1104 (1955).
[14] Gultyaev P.V., Petrov A.V.: Sov. Phys. Solid State **1**, 330 (1959).
[15] Shoemake G.E., Rayne J.A., Ure R.W.: Phys. Rev. **185**, 1046 (1969).
[16] Dyck J. S., Chen W., Uher C., Drašar Č., Lošťák P.: Phys. Rev. B **66**, 125206 (2002).
[17] Klemens P.G.: Proc. Phys. Soc. London, A **68**, 1113 (1955).
[18] Abeles B.: Phys. Rev. **131**, 1906 (1963).
[19] Shannon R.D.: Acta Crystallographica A **32**, 751 (1976).
[20] Pauling L.: *The Nature of the Chemical Bond*, p.155 , Cornell University Press, 1961.
[21] Glassenbrenner G.A., Slack G.A.: Phys. Rev.**134**, 1058 (1964).
[22] Parrott J.E., Stuckes A.D.: *Thermal Conductivity of Solids*, p. 68, Pion Limited, London, 1975.
[23] Dyck J.S., Švanda P., Lošťák P., Horák J., Chen W., Uher C.: J. Appl. Phys. **94**, 7631 (2003).
[24] Horák J., Drašar Č., Novotný R., Karamazov S., Lošťák P.: Phys. Stat. Sol. (a) **149**, 549 (1995).
[25] Starý Z., Beneš L., Horák J.: Phys. Stat. Sol. (a) **109**, 93 (1988).
[26] Plecháček T., Horák J.: J. Sol. State Chem. **145**, 297 (1999).
[27] Lošťák P., Drašar Č., Krejčová A., Beneš L., Dyck J.S., Chen W., Uher C.: J. Cryst. Growth **222**, 565 (2001).
[28] Van Itterbeek A., Van Deynse N., Herinckx C.: Physica **32**, 2123 (1966).
[29] Ohno H.: J. Magn. Magn. Mater. **200**, 110 (1999).
[30] Escorne M., Mauger A., Tholence J. L., Triboulet R.: Phys. Rev. B **29**, 6306 (1984).
[31] Dyck J.S., Chen W., Hájek P., Lošťák P., Uher C.: Physica B **312-313**, 820 (2002).
[32] Dyck J.S., Chen W., Hájek P., Lošťák P., Uher C.: Phys. Rev. B **65**, 115212 (2002).
[33] Stoner E.C., Wohlfarth E.P.: Philos. Trans. R. Soc. London, Ser. A **240**, 599 (1948).
[34] von Molnár S., Kasuya T.: Phys. Rev. Lett. **21**, 1757 (1968).
[35] Hurd C.M.: *The Hall Effect in Metals and Alloys*, p. 153, Plenum, New York, 1972.
[36] Dyck J.S., Drašar Č., Lošťák P., Uher C.: Phys. Rev. B , in press.
[37] Yuldashev S.U., Im H., Yalishev V.S., Park C.S., Kang T.W., Lee S., Sasaki Y., Liu X., Furdyna J.K.: Appl. Phys. Lett. **82**, 1206 (2003).
[38] Wojtowicz T., Cywinski G., Lim W.L., Liu X., Dobrowolska M., Furdyna J. K., Yu K.M., Walukiewicz W., Kim G.B., Cheon M., Chen X., Wang S.M., Luo H.: Appl. Phys. Lett. **82**, 4310 (2003).
[39] Kulbachinskii V.A., Kaminskii A. Yu., Kindo K., Narumi Y., Suga K., Lošťák P., Švanda P.: JETP Letters **73**, 352 (2001).

[40] Pearton, S.J., Abernathy C.R., Norton D.P., Hebard A. F., Park Y.D., Boatner L.A., Budai J.D.: Mater. Sci. Eng. R **40**, 137 (2003).
[41] Sato K., Yoshida H.K.: Semicond. Sci. Technol. **17**, 367 (2002).
[42] Dietl T.: Semicond. Sci. Technol. **17**, 377 (2002).
[43] Story T., Galazka R.R., Frankel R.B., Wolf P.A.: Phys. Rev. Lett. **56**, 777 (1986).
[44] Furdyna J.K.: J. Appl. Phys. **64**, R29 (1988).
[45] Ohno H.: J. Magn. Magn. Mater. **200**, 110 (1999).